Determining Graphene and Substrate Quality from the Coupled Hall Mobility Measurements and Theoretical Modeling

K. Japec[1], M. Matić[1], R. Lukose[2], M. Lisker[2,3], M. Lukosius[2,**] and M. Poljak[1,*]

[1]Computational Nanoelectronics Group, Micro and Nano Electronics Laboratory, Faculty of Electrical Engineering and Computing, University of Zagreb, 10000 Zagreb, Croatia

[2]2D Materials Group, IHP–Leibnitz Institute for High Performance Microelectronics, 15236 Frankfurt (Oder), Germany

[3]Technical University of Applied Science Wildau, 15745 Wildau, Germany

[*]E-mail: mirko.poljak@fer.hr, [**]E-mail: lukosius@ihp-microelectronics.com

***Abstract*—An increase of mobility up to ~2600 cm²/Vs is observed in graphene by Hall bar characterization within the temperature range from 40 K to 300 K. The increasing trend is attributed to Coulomb scattering by employing theoretical modeling based on the momentum relaxation time approximation of the Boltzmann transport equation. We also find that at room temperature and for higher charge densities additional mechanisms such as lattice defect and/or substrate corrugation scattering become important and restrict the mobility down to only ~200 cm²/Vs and carrier mean free paths well under ~35 nm.**

Keywords—graphene, mobility, scattering rate, Coulomb impurity, corrugations, defects, surface roughness, momentum relaxation time (MRT) approximation

I. Introduction

The high carrier mobility and its atomically-thin crystal structure make graphene a promising two-dimensional (2D) material for applications in electronics, photonics and other engineering fields [1]–[3]. However, successful integration of graphene monolayers into CMOS is limited by the lack of cost-efficient growth methods on CMOS compatible substrates. Recently, an appropriate substrate for growing graphene was found in Ge, mainly due to very low solubility of carbon [4]. While Ge(110) is superior in terms of graphene grain formation and mobility [4], Ge(001) is more compatible with the standard Si(001) wafers and process flow [5], [6]. For graphene growth on Ge(001) substrates, carrier mobility ranging from a few ~100 cm²/Vs [7] to ~10,000 cm²/Vs [8] at room temperature and low carrier density is reported. However, in the latter case it is unclear what limits the mobility at low densities, and transport features at high carrier densities remained unknown.

Complementary to experiments, theoretical modeling and numerical simulations of carrier transport can provide physical insights into material and device properties [9]–[11], which allows an optimization of processing parameters. In this work, we employ the momentum relaxation time (MRT) approximation of the Boltzmann transport equation to calculate electron/hole mobility for all relevant scattering mechanisms ranging from phonon, over Coulomb to substrate roughness scattering. Calibration on temperature-dependent measurements allows the extraction of graphene and substrate quality parameters such as lattice defect or charged impurity density. We report that the mobility increases with increasing temperature from 40 K to 300 K, which is attributed to the dominant impact of Coulomb scattering, and that it reaches ~2600 cm²/Vs at $T = 300$ K, being limited by substrate roughness/corrugations and/or defect scattering within graphene.

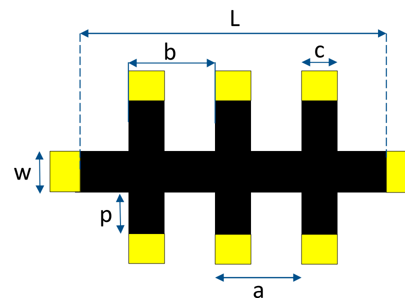

Fig. 1. Schematic illustration of 8-contact Hall bar devices. $L = 20$ µm, $a = 5$ µm, $b = 5$ µm, $c = 2$ µm, $w = 6$ µm, $p = 2$ µm.

II. Methodology

A. Fabrication and Characterization

The fabrication process of 8-contact Hall bar devices (Fig. 1) from chemical vapor deposition (CVD) grown graphene involves several steps. Firstly, a layer of graphene is grown on a Ge/Si(001) substrate using the CVD technique at 885 °C. The graphene layer is then transferred onto a target substrate (SiO_2 in this work) using a polymer-based electrochemical delamination transfer method. Next, lithography is used to define the device geometry, followed by etching of the unwanted graphene using reactive ion etching (RIE) process. After graphene is patterned, Au metal contacts are deposited using a thermal evaporation technique, followed by lift-off procedure of the polymer resist. Finally, the devices were annealed at

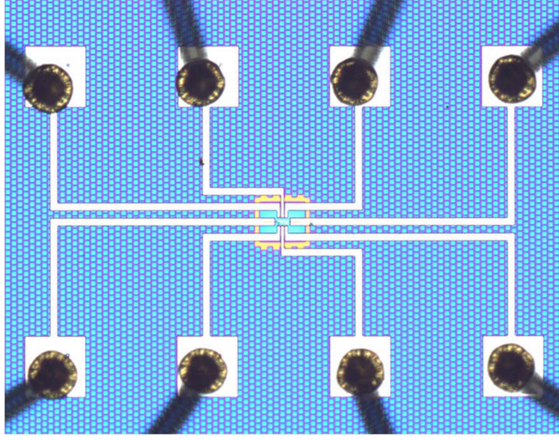

Fig. 2. Photograph under an optical microscope of the 8 contact Hall bar device under study.

250 °C temperature to improve the contact resistance between the metal contacts and the graphene monolayer.

Hall bar measurements in the range of 40 – 300 K in the magnetic field up to 1 Tesla were used to investigate the electronic and transport properties of graphene Hall bar devices (Fig. 2). The Hall effect occurs when a magnetic field is applied perpendicularly to the direction of current flow in a conductor. This creates a transverse voltage across the conductor, which is proportional to the strength of the magnetic field and the carrier density of the material. By measuring the Hall voltage as a function of magnetic field strength and temperature, information about the carrier mobility, carrier sheet density, and carrier type was extracted. The range of 40 – 300 K is chosen to study the material behavior at both room temperature and lower temperatures where quantum mechanical effects related to Dirac transport become more pronounced.

B. *Theory and Numerical Simulations*

The main goal of this paper is to find the mechanisms responsible for the increase of mobility with temperature in the fabricated graphene samples, and to estimate quality parameters of graphene and substrate upon which it is deposited. We calculate carrier mobility by employing the MRT approximation of the Boltzmann transport equation [9], [10], [12], thus building on our previous work [13], especially concerning quasi-one-dimensional graphene nanoribbons [14], [15]. Mobility in graphene is limited by various scattering mechanisms that are more or less significant for the overall transport depending on e.g. temperature and carrier density. In this work, we implement all relevant mechanisms such as scattering on intrinsic acoustic phonons (AP) [16] and optical phonons (OP) [10] in graphene, surface optical phonons (SOP) [17] that originate from the dielectric substrate, Coulomb (CO) scattering originating from charged impurities on the substrate [11], atomic-scale lattice defect (DEF) scattering [18] from missing carbon atoms, and surface roughness or substrate corrugation (COR) scattering [11].

The expressions for MRT spectra are given in the literature, and here we explicitly define only the two most relevant ones. For Coulomb impurity scattering the energy-dependent CO scattering rate is given as in [11], i.e.

$$\frac{1}{\tau_{CO}} = \frac{N_{imp}}{4\pi\hbar E}\left(\frac{Ze^2}{\varepsilon}\right)^2 \int_0^{\pi/2} d\theta \frac{\sin^2(\theta)\, e^{-k\sin(\theta)d_s}}{\left[\sin(\theta)+\frac{q_S}{2k}\right]^2} \tag{1}$$

where N_{imp} represents the aerial density of charged impurities, q_S is the screening wave vector, while d_S is the distance between impurities, i.e. the substrate, and the graphene sheet. The screening function considered in this work is static and equals

$$q_s = \frac{e^2 E(k)}{2\pi\varepsilon(\hbar v_F)^2} \tag{2}$$

where ε is graphene dielectric constant, and v_F is the Fermi velocity in graphene. Screening is taken into account for the CO and SOP MRT calculations. Another important scattering mechanism defined here is the substrate corrugation scattering which is assumed to arise after graphene sheet is deposited on the (oxide) substrate that is not perfectly flat. The energy-dependent COR scattering rate is given as in [11], i.e.

$$\frac{1}{\tau_{COR}(E)} = \frac{2k}{v_F}\left(\frac{\Delta L e^2 n_S}{2\hbar\varepsilon}\right)\frac{1}{\sqrt{1+k^2L^2}} E\left(\frac{kL}{\sqrt{1+k^2L^2}}\right) \tag{3}$$

where n_S is the gate-induced sheet carrier density, Δ is the rms height and L is the correlation length for the corrugations or roughness of the substrate. In the experiments, the n_S is found from the current, magnetic field and Hall voltage, whereas in the simulations the n_S is defined by Fermi level shift in graphene.

After each MRT spectrum is known, the mobility limited by each of the different mechanisms is calculated by energy averaging [10], [14], [19]. For example, the COR-limited mobility is designated as μ_{COR}, the SOP-limited mobility is designated as μ_{SOP}, and so on. After calculating these components, the total mobility is calculated using the Matthiessen's rule defined as

$$\frac{1}{\mu_{TOT}} = \sum_m \frac{1}{\mu_m} . \tag{4}$$

where m presents individual scattering mechanisms. Unless stated otherwise, the constants and parameters used in the simulations are those defined in the cited literature.

III. Results and Discussion

Figure 3 shows the fitting between the measured and simulated mobility in the temperature range from 40 K to 300 K. The simulated curve is obtained for the charge carrier density $n = 1.867 \times 10^{12}$ cm^{-2}, close to carrier density maintained in Hall measurements. Other simulation parameters set to achieve the fitting in Fig. 3 are as follows: density of impurities $N_{imp} = 2.18 \times 10^{11}$ cm^{-2} (for CO scattering), defect concentration $N_{def} = 0.18 \times 10^{10}$ cm^{-2} (for DEF scattering), and rms height $\Delta = 1.3$ nm and the correlation length $L = 2$ nm (for COR scattering). The simulated mobility matches the experimental data well, especially for $T > 100$ K, while for lower temperatures the mismatch is smaller than 8.5%. We attribute this difference visible for $T < 100$ K to simplifications in scattering modeling such as equipartition approximation for acoustic phonons, absence of an incomplete ionization model, using a very simple screening model etc.

Generally, mobility increases with temperature with the values of the measured mobility ranging from 2226 cm^2/Vs to 2626 cm^2/Vs, while the simulated mobility being in the range from 2390 cm^2/Vs at $T = 40$ K to 2640 cm^2/Vs at $T = 300$ K. Given this increase with temperature, only two mechanisms could be responsible for the overall mobility behavior, i.e. CO and/or COR scattering. In the case of CO scattering, increasing T increases the average kinetic energy of carriers, which in turn decreases CO-MRT rate as given in Eq. (1), increases screening according to Eq. (2), with both effects resulting in μ_{CO} increase with temperature. In order to clarify this issue, in Fig. 4 we plot the impact of temperature increase on the individual mechanisms and we can see how they contribute to the total mobility according to the Matthiessen's rule. Clearly, CO scattering, followed by COR scattering, exhibit the strongest impact on the total mobility, and are responsible for the overall increase of μ_{TOT} with increasing temperature. In contrast, other mechanisms such as AP, OP, SOP and DEF scattering become stronger at higher temperatures. If, for example, SOP or DEF scattering become dominant in certain graphene samples, that would be seen from a moderately decreasing μ_{TOT} with increasing temperature. The μ_{OP} is several orders of magnitude higher than mobilities limited by other sources of scattering and is, therefore, of little significance for electron transport in our samples.

It is worth looking into MRT spectra to investigate the relative influence of different mechanisms of scattering at room temperature, as reported in Fig. 5 for $T = 300$ K. We observe that at low (kinetic) energies the strongest mechanism is the CO scattering with rates as high as ~10^{14} s^{-1}, whereas at energies $E > 0.17$ eV the COR scattering dominates over all other scattering mechanisms. For $E > 0.5$ eV the CO scattering becomes the weakest mechanism, with the lowest rate of ~4×10^{11} s^{-1} at $E = 1$ eV, and the weakest influence on μ_{TOT}. We note that for all spectra, except for the CO mechanism, the scattering rate increases with energy and most mechanisms reach the

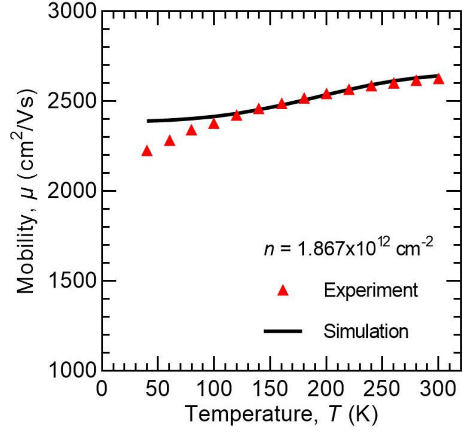

Fig. 3. Comparison between the measured and simulated temperature-dependent electron mobility in the range 40 – 300 K.

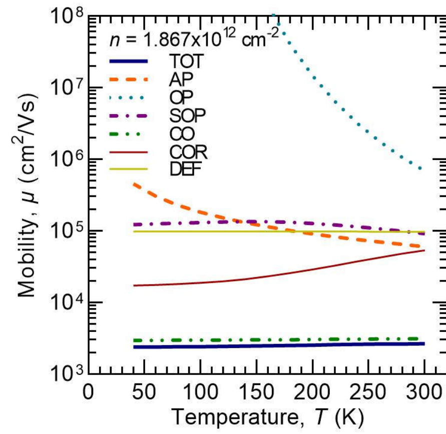

Fig. 4. Temperature-dependence of individual mobilities limited by different scattering mechanisms.

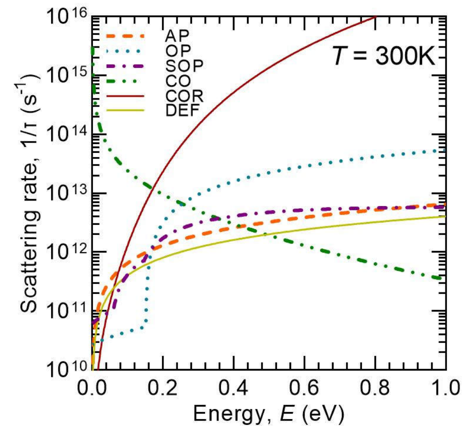

Fig. 5. Scattering rate spectra at 300 K for all the included scattering mechanisms.

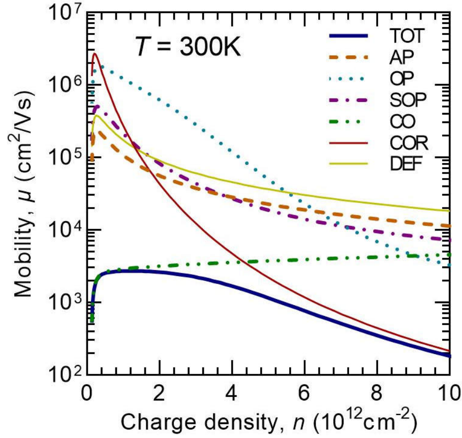

Fig. 6. Mobility in graphene vs. charge density at 300 K for all the included scattering mechanisms.

rate of ~5×10^{12} s^{-1} at high energies. In turn, the increasing scattering rate results in mobility decrease with increasing kinetic energy, except for the CO scattering that behaves oppositely.

The previous assertions about the scattering spectra are confirmed in Fig. 6 where we show the mobility as a function of carrier charge density for $T = 300$ K. When n increases, the total mobility first increases up to 2708 cm^2/Vs at $n = 1.26 \times 10^{12}$ cm^{-2} and after that point it starts to decrease. In this point of the local mobility maximum the mean free path (MFP) equals $\hbar\mu\sqrt{\pi n}/q \approx 35.5$ nm. As shown in Fig. 6, at low carrier concentrations the limiting factor is the CO scattering and for the higher concentrations the COR scattering is dominant. Hence, increasing μ_{CO} for low n, and decreasing μ_{COR} for high n determines the μ_{TOT}-n characteristic, at least in the current constellation of simulation parameters. The only other way that could provide a decreasing μ_{TOT} with increasing n, as reported in all experiments so far [7], [8], [20], [21], is to assume COR scattering to be negligible, and DEF scattering strong at high kinetic energies or carrier densities, well above the initially assumed value of $N_{def} = 0.18 \times 10^{10}$ cm^{-2}, e.g at about ~10^{11} cm^{-2}. The increased N_{def} would infer a rather short average distance between individual defects of ~32 nm, assuming their distribution in a perfectly square arrangement. Hence, $N_{def} = 10^{11}$ cm^{-2} seems unrealistically high when compared to previously fabricated graphene by the same group at IHP [6]–[8], and this should be further analyzed by a detailed Raman spectroscopy study.

Finally, while the Hall measurements are done at different temperatures, but at the same carrier density, the well-calibrated transport model presented here allows us to extract the mobility at technologically more relevant densities up to $n \sim 10^{13}$ cm^{-2}. At these values corresponding to e.g. strong inversion in field-effect transistors (FETs), the simulated mobility equals 200 cm^2/Vs. While this value is orders of magnitude lower than in suspended graphene samples at low temperatures [21], it is much higher than the field-effect mobility measured or simulated in ultra-thin semiconductor layers of comparable thickness [22], [23], [13], [24]. Additionally, the MFP in this case equals $\hbar\mu\sqrt{\pi n}/q \approx 7.4$ nm, which is comparable to channel length in modern CMOS FETs and should allow for at least quasi-ballistic carrier transport.

IV. Conclusions

The quality of graphene and substrate upon which it is grown are analyzed by a coupled experimental and theoretical study of carrier mobility. The Hall bar structures were characterized in the temperature range from 40 K to 300 K at moderate charge density, whereas MRT approximation of the Boltzmann transport equation is used to theoretically calculate scattering spectra of all relevant scattering mechanisms. The experiments reveal an increasing μ_{TOT} with increasing temperature, which is reproduced by simulations and attributed to CO scattering with $N_{imp} \approx 2.2 \times 10^{11}$ cm^{-2} over the entire temperature range. Regarding charge density dependence and room temperature characteristics, the theory predicts either strong COR scattering with high roughness/corrugation amplitudes ($\Delta = 1.3$ nm, $L = 2$ nm) or a high density of lattice defects within the graphene monolayer ($N_{def} > 10^{11}$ cm^{-2}) to achieve a good match with experimental data. Therefore, additional improvements are needed in the transfer process to reduce defect density and/or graphene corrugations if mobilities greater than 2700 cm^2/Vs and MFPs above 35 nm are needed.

Acknowledgments

This work was supported by the Croatian Ministry of Science and Education and the German Academic Exchange Service (DAAD) through the Croatia-Germany Bilateral Project GRONGER. M. P. also acknowledges partial support by the Croatian Science Foundation under the project CONAN2D (Grant No. UIP-2019-04-3493).

References

[1] K. S. Novoselov *et al.*, "Electric Field Effect in Atomically Thin Carbon Films," *Science*, vol. 306, no. 5696, pp. 666–669, Oct. 2004, doi: 10.1126/science.1102896.

[2] F. Bonaccorso, Z. Sun, T. Hasan, and A. C. Ferrari, "Graphene photonics and optoelectronics," *Nature Photonics*, vol. 4, no. 9, pp. 611–622, Aug. 2010, doi: 10.1038/nphoton.2010.186.

[3] G. Fiori *et al.*, "Electronics based on two-dimensional materials," *Nat. Nanotechnol.*, vol. 9, no. 10, pp. 768–779, Oct. 2014, doi: 10.1038/nnano.2014.207.

[4] J.-H. Lee *et al.*, "Wafer-Scale Growth of Single-Crystal Monolayer Graphene on Reusable Hydrogen-Terminated Germanium," *Science*, vol. 344, no. 6181, pp. 286–289, Apr. 2014, doi: 10.1126/science.1252268.

[5] I. Pasternak *et al.*, “Large-area high-quality graphene on Ge(001)/Si(001) substrates,” *Nanoscale*, vol. 8, no. 21, pp. 11241–11247, May 2016, doi: 10.1039/C6NR01329E.

[6] M. Lukosius *et al.*, “Metal-Free CVD Graphene Synthesis on 200 mm Ge/Si(001) Substrates,” *ACS Appl. Mater. Interfaces*, vol. 8, no. 49, pp. 33786–33793, Dec. 2016, doi: 10.1021/acsami.6b11397.

[7] M. Lisker *et al.*, “Processing and integration of graphene in a 200 mm wafer Si technology environment,” *Microelectronic Engineering*, vol. 205, pp. 44–52, Jan. 2019, doi: 10.1016/j.mee.2018.11.007.

[8] J. Aprojanz *et al.*, “High-Mobility Epitaxial Graphene on Ge/Si(100) Substrates,” *ACS Appl. Mater. Interfaces*, vol. 12, no. 38, pp. 43065–43072, Sep. 2020, doi: 10.1021/acsami.0c10725.

[9] M. Lundstrom, *Fundamentals of Carrier Transport*, 2nd ed. New York, NY, USA: Cambridge University Press, 2000.

[10] R. S. Shishir and D. K. Ferry, “Intrinsic mobility in graphene,” *J. Phys.: Condens. Matter*, vol. 21, no. 23, p. 232204, Jun. 2009, doi: 10.1088/0953-8984/21/23/232204.

[11] R. S. Shishir, F. Chen, J. Xia, N. J. Tao, and D. K. Ferry, “Room temperature carrier transport in graphene,” *J Comput Electron*, vol. 8, no. 2, pp. 43–50, Jun. 2009, doi: 10.1007/s10825-009-0278-y.

[12] M. Bresciani, P. Palestri, D. Esseni, and L. Selmi, “Simple and efficient modeling of the E–k relationship and low-field mobility in Graphene Nano-Ribbons,” *Solid-State Electronics*, vol. 54, no. 9, pp. 1015–1021, Sep. 2010, doi: 10.1016/j.sse.2010.04.038.

[13] M. Poljak, V. Jovanovic, D. Grgec, and T. Suligoj, “Assessment of Electron Mobility in Ultrathin-Body InGaAs-on-Insulator MOSFETs Using Physics-Based Modeling,” *IEEE Transactions on Electron Devices*, vol. 59, no. 6, pp. 1636–1643, Jun. 2012, doi: 10.1109/TED.2012.2189217.

[14] M. Poljak, T. Suligoj, and K. L. Wang, “Influence of substrate type and quality on carrier mobility in graphene nanoribbons,” *Journal of Applied Physics*, vol. 114, no. 5, p. 053701, Aug. 2013, doi: 10.1063/1.4817077.

[15] M. Poljak, K. L. Wang, and T. Suligoj, “Variability of bandgap and carrier mobility caused by edge defects in ultra-narrow graphene nanoribbons,” *Solid-State Electronics*, vol. 108, pp. 67–74, Jun. 2015, doi: 10.1016/j.sse.2014.12.012.

[16] E. H. Hwang and S. Das Sarma, “Acoustic phonon scattering limited carrier mobility in two-dimensional extrinsic graphene,” *Phys. Rev. B*, vol. 77, no. 11, p. 115449, Mar. 2008, doi: 10.1103/PhysRevB.77.115449.

[17] I.-T. Lin and J.-M. Liu, “Surface polar optical phonon scattering of carriers in graphene on various substrates,” *Appl. Phys. Lett.*, vol. 103, no. 8, p. 081606, Aug. 2013, doi: 10.1063/1.4819395.

[18] D. K. Ferry, “Short-range potential scattering and its effect on graphene mobility,” *J Comput Electron*, vol. 12, no. 2, pp. 76–84, Jun. 2013, doi: 10.1007/s10825-012-0431-x.

[19] D. K. Ferry, S. M. Goodnick, and J. Bird, *Transport in Nanostructures*, 2nd ed. New York, NY, USA: Cambridge University Press, 2009.

[20] V. E. Dorgan, M.-H. Bae, and E. Pop, “Mobility and saturation velocity in graphene on SiO2,” *Applied Physics Letters*, vol. 97, no. 8, pp. 082112-082112–3, Aug. 2010, doi: doi:10.1063/1.3483130.

[21] K. I. Bolotin *et al.*, “Ultrahigh electron mobility in suspended graphene,” *Solid State Communications*, vol. 146, no. 9–10, pp. 351–355, Jun. 2008, doi: 10.1016/j.ssc.2008.02.024.

[22] K. Uchida, H. Watanabe, A. Kinoshita, J. Koga, T. Numata, and S. Takagi, “Experimental study on carrier transport mechanism in ultrathin-body SOI nand p-MOSFETs with SOI thickness less than 5 nm,” in *IEDM Tech. Dig.*, IEEE, 2002, pp. 47–50. doi: 10.1109/IEDM.2002.1175776.

[23] D. Esseni, A. Abramo, L. Selmi, and E. Sangiorgi, “Physically based modeling of low field electron mobility in ultrathin single- and double-gate SOI n-MOSFETs,” *IEEE Trans. Electron Devices*, vol. 50, no. 12, pp. 2445–2455, Dec. 2003, doi: 10.1109/TED.2003.819256.

[24] S. Krivec, M. Poljak, and T. Suligoj, “Electron mobility in ultra-thin InGaAs channels: Impact of surface orientation and different gate oxide materials,” *Solid-State Electronics*, vol. 115, no. Part B, pp. 109–119, Jan. 2016, doi: 10.1016/j.sse.2015.08.009.